Infrared-Active Vibrational Modes of Single-Walled Carbon Nanotubes

U. J. Kim,[1] X. M. Liu,[1] C. A. Furtado,[2] G. Chen,[1] R. Saito,[3] J. Jiang,[3] M. S. Dresselhaus,[4] and P. C. Eklund[1,*]

[1]*Department of Physics, The Pennsylvania State University, University Park, Pennsylvania 16802, USA*
[2]*Centro de Desenvolvimento da Tecnologia Nuclear—CDTN/CNEN, Belo Horizonte, MG, Brazil*
[3]*Department of Physics, Tohoku University and CREST JST, 980-8578, Sendai Japan*
[4]*Department of Physics, MIT, Cambridge, Massachusetts 02139, USA*

(Received 22 September 2004; published 3 October 2005)

The IR-active vibrational modes of single-walled carbon nanotubes have been observed by optical transmission through thin films of bundled nanotubes. Because IR-active chemical functional groups, e.g., −COOH, −OH, might be attached to the tube walls and contribute additional spectral features, we have also studied the effects of chemical purification and long-term high-temperature vacuum annealing on the IR spectrum. Through comparison with theory, we are able to assign much of the sharp stucture observed in our IR spectra.

DOI: 10.1103/PhysRevLett.95.157402 PACS numbers: 78.67.Ch, 78.30.Na

Despite the fact that single-walled carbon nanotubes (SWNTs) have been produced in the laboratory and widely studied for more than ten years [1–4], relatively little is known about the infrared (IR)-active vibrational modes of this important macromolecule. In contrast, Raman scattering has been used almost from the time of the discovery of the SWNT to probe the vibrational modes of carbon nanotubes [5,6]. The Raman studies have been facilitated by a strong resonance in the scattering cross section, and this resonance has been identified with interband transitions between mirror image van Hove singularities (vHs) in the quasi-1D electronic density of states (DOS) [5,6]. Recently, this interpretation of the resonance has been called into question, however, as a convincing set of experiments [7] and theoretical calculations [8–10] indicate that strong excitonic effects may overwhelm the interband dipole activity near the band edges.

SWNT IR vibrational modes, on the other hand, are much more difficult to detect. The difficulty stems, in part, from the fact that SWNTs do not support a static dipole moment, and must therefore generate a dynamic dipole moment, which is usually much weaker. An earlier report of phonon modes observed by reflectance from unpurified powder containing SWNTs and graphitic nanocarbons produced by the arc process has appeared [11]. Two dominant structures were observed after the derivative of the SWNT powder diffuse reflectance was inspected, one band at $\sim$868 cm^{-1} and the other at $\sim$1590 cm^{-1} (close to A_{2u}, and E_{1u} modes of graphite, respectively).

In this Letter, we report the first systematic experimental attempts to observe the IR-active modes of SWNTs. In concert with theoretical calculations on freestanding SWNTs (i.e., without nanotube-nanotube, or nanotube-solid surface interactions), we are able to assign much of the sharp structure in the IR spectra of purified and annealed SWNTs to one- and two-phonon lattice mode bands.

Bundles of typically $\sim$100 or more SWNTs with tube diameters in the range $1.2 \leq d \leq 1.6$ nm were grown by the electric arc method (CarboLex, Inc.). The material was purified via a three-step process [12]. The last step involved a 4–24 h vacuum anneal in $\sim 1 \times 10^{-7}$ Torr at 1100 or 1400 °C. For the IR studies, transparent bundled nanotube films were deposited from a 2-propanol suspension onto ZnSe substrates and vacuum degassed at 200 °C to remove residual 2-propanol. Room temperature transmission spectra on these films were collected using a BOMEM DA3+ Fourier transform infrared spectrometer employing a cooled HgCdTe (MCT) detector with a spectral resolution $\sim$4 cm^{-1}.

The SWNT structure can be classified according to whether the tube is achiral {i.e., "zigzag" $(n, 0)$ or "armchair" (n, n)}, or chiral $\{(n, m); n \neq m\}$ [4]. Chiral nanotubes can exhibit very large (i.e., long) one-dimensional (1D) unit cells compared to achiral tubes of the same diameter. It is indeed a surprising result from the group theory of nanotubes [13,14] that the number of IR- and Raman-active modes in a chiral tube is almost the same as that for an achiral tube with a much shorter unit cell. In a graphene sheet, the crystal symmetry forbids a $q = 0$ IR-active optical phonon. However, this rule is broken by the cylindrical boundary condition of the SWNT. Based on group theory, we can say that between 5 and 13 $q = 0$ modes are IR active, depending on the chirality of the specific tube [4]. A different set of selection rules has been presented in Ref. [15]. The difference between these two sets of selection rules lies in a disagreement over the correct set of covering operations for the specific (n, m) nanotube [4]. In an IR experiment, all the tubes in the ensemble can be probed at the same time, whereas the resonance in the Raman cross section allows only a few (n, m) to be probed in the same experiment.

Lattice dynamics calculations show that modes below $\sim$400 cm^{-1} exhibit significant radial character, whereas modes above $\sim$1100 cm^{-1} exhibit primarily tangential C-atom displacement [4,13,14]. Two-phonon Raman and IR excitations exist above $\sim$1600 cm^{-1}. On the other hand, vibrational modes of functional (chemical) groups,

e.g., −COOH, −OH, C-H, may also be present [16]. It is therefore important to have some experimental basis for the assignment of the observed IR structure to intrinsic nanotube modes. Our approach to this problem has been to study the evolution of the $T = 300$ K IR spectrum in a series of purified samples that have each been exposed to a successively higher temperature vacuum anneal (HTVA). Eventually, ($T \geq 1200\,^{\circ}$C [16]) most of these groups have desorbed as gas, and their vibrational mode intensity is expected to decrease significantly as the temperature is increased from 600 °C to 1200 °C.

In Fig. 1, we display the $T = 300$ K optical density (OD) of several SWNT films. The inset at the top of the figure shows the OD on a log frequency scale from the Far IR to the UV for a purified sample with HTVA = 1100 °C. All the strong broad features in the inset are due to electronic transitions, and their position is in good agreement with the literature [17–19]. The broad peak (labeled E_c) at ~200 cm^{-1} is consistent with electronic transitions across a range of curvature-induced small energy gaps [17]. Between ~4000 and ~18 000 cm^{-1}, three bands are observed labeled (E_1^s, E_{22}^s, and E_1^m). They have been observed previously and identified with electronic transitions across the much larger "chirality" gaps $E_{ij}^{s(m)}$ [18,19]. However, as we discussed above, strong excitonic effects need to be considered in the interpretation of this structure. Finally, on the basis of band structure calculations [18] and the observed dielectric function of graphite [20], the strongest peak at ~35 000 cm^{-1} in Fig. 1 (labeled M) is identified with the "cylindrical analog" of the $\pi - \pi^*$ electronic interband absorption of a graphene sheet.

The relatively weak IR-active vibrational structure associated with the nanotube film is barely visible on the OD scale of the inset. In Fig. 1(e) we display the mid-IR spectrum of a purified sample with HTVA = 1400 °C. To enhance the visibility of the sharp structure, we first subtract the background (cubic polynomial) identified with the electronic contribution [dotted line in Fig. 1(e)]. The difference spectrum is shown in Fig. 1(d).

The parameters of the cubic polynomial are chosen to produce a flat mid IR spectrum after subtraction. The polynomials we have used do not produce the variety of 10–20 cm^{-1} wide structures in the difference spectra. Other vibrational (difference) spectra labeled (a), (b) and (c) (see bottom of Fig. 1) were obtained similarly. They correspond, respectively, to (a) as-delivered SWNT material vacuum degassed at 200 °C, (b) after purification and vacuum degassing at 200 °C, and (c) after purification and HTVA = 1100 °C. The horizontal bars at the bottom of Fig. 1 identify the typical frequency intervals in which IR-active modes occur for the specified chemical groups. It is clear that some of the strong broad bands in the difference spectrum for the as-delivered and chemically-processed SWNT material match up well with these bars [16]. Because many of these IR bands can be removed with HTVA, they can be assigned to the specified chemical

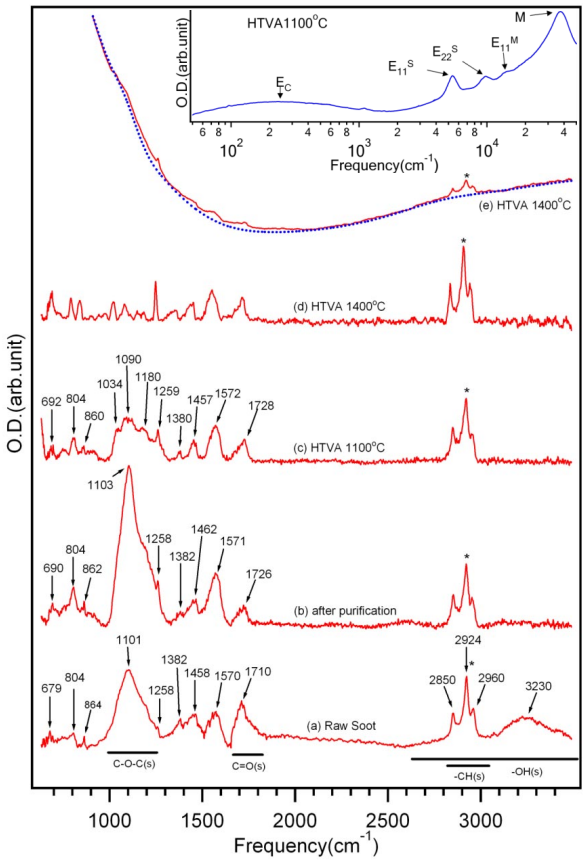

FIG. 1 (color online). Difference spectra for raw and purified SWNT samples annealed at various temperatures: (a) raw soot SWNT material, (b) after purification, (c) after purification and HTVA = 1100 °C, (d) after purification and HTVA = 1400 °C. Spectrum (e) is that of a sample with HTVA = 1400 °C and a polynomial fit to a smooth background (dotted line). Inset: the entire spectrum of a sample exposed to HTVA = 1100 °C. The asterisk (*) indicates a triplet, which is a spectral artifact.

functional groups indicated; they are not SWNT modes [16]. For example, in spectrum (a), a very broad band with a maximum near 3200 cm^{-1} can be identified with −OH from carboxylic acid groups attached either to SWNTs or to other nanocarbons present in the as-delivered material. After chemical purification, this band is reduced in strength; it disappears completely after HTVA = 1100 °C. Also, the feature at ~1710 cm^{-1}, which is near the C = O stretching modes, is diminished by our purification, yet we see a growth of the feature near the C-O-C stretching mode region after chemical processing. Most of the IR activity identified with chemical functional groups in Fig. 1(a) can be removed by HTVA = 1400 °C, except for the 2900 cm^{-1} triplet. This triplet has been observed previously and identified with C-H$_n$ functional groups introduced by atomic hydrogen generated in cold plasma [21]. We believe that the 2900 cm^{-1} triplet is associated with hydrocarbon contamination in our spectrometer [16]. The broad asymmetric band at 1730 cm^{-1} in (d) has also survived HTVA = 1400 °C. It lies above the maximum

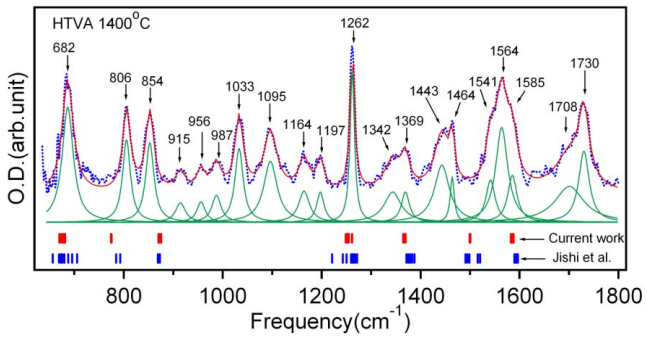

FIG. 2 (color online). Spectra of a purified SWNT sample with HTVA = 1400 °C. Calculated 1st order-allowed $q = 0$ modes of SWNTs in the diameter range of 1.2–1.6 nm from current work and Jishi *et al.* are also shown [13].

frequency for one-phonon excitation in SWNTs. Although this feature has a frequency close to that observed for IR bands in organic compounds with $-C=O$ stretching modes, we find that the 1710 cm^{-1} band changes very little with purification or annealing: it does undergo slight changes of shape, and is reduced somewhat in intensity and upshifts by ~20 cm^{-1}, and it is still present after HTVA = 1400 °C. Therefore, the ~1730 cm^{-1} feature in Fig. 1(e) appears to be a 2-phonon SWNT excitation.

In Fig. 2, we expand the vibrational spectrum of a HTVA = 1400 °C film [Fig. 1(d)] in the range 600–1800 cm^{-1}, and fit the peaks to Lorentzians. We believe this film represents the most intrinsic SWNT sample in this study. The thin solid line through the data is the composite fit, and the individual Lorentzians are displaced below the spectrum for clarity. Their full width at half maxima (FWHM) are in the range 10–20 cm^{-1}.

Of the 18 narrow bands in Fig. 2 in the 1st order region (below 1600 cm^{-1}), 8 are close in frequency to IR modes calculated for achiral SWNTs; the IR frequencies from our current model calculations on tubes of similar diameter appear as vertical bars below this spectrum; below these bars are another set of bars representing the IR frequencies calculated by Jishi *et al.* previously [13] for achiral tubes with diameters similar to our sample. As Jishi *et al.* have shown, the diameter dependence of the frequencies for $q = 0$ Raman- and IR-active modes above ~1000 cm^{-1} is relatively unimportant. So, for the high frequency modes, the fact that we have a chirality-diameter distribution does not present as serious a complication for the spectral analysis as one might expect. Based on the proximity in frequency between many of the observed narrow IR features in Fig. 2 below 1600 cm^{-1} with calculated $q = 0$ modes, we feel that we can make some tentative assignments of the bands observed in Fig. 2 at this stage. The results of these identifications are summarized in Table I.

For this work, we have developed a new approach for calculating phonon dispersion for specific (n, m) tubes and wave vector q [22]. The rotational symmetry around the nanotube axis for the calculation of phonon dispersion is adopted. Thus a $6N \times 6N$ dynamical matrix is changed to N 6×6 small dynamical matrixes, where N is the number of atoms in a primitive cell. This reduces the computational time significantly, but no changes in the numerical results are obtained in several specific cases examined closely. The force constants have been modified to reproduce the resonant Raman scattering [23,24] and the inelastic x-ray scattering for graphite [25], especially around the K point of the 2D graphene Brillouin zone (BZ). The force constants used by Jishi *et al.* were fitted to neutron scattering data on graphite, but these data were relevant between the

TABLE I. Comparison of experimental and theoretical IR structure.

Experiment[a] (cm^{-1})	Theory (cm^{-1})	Assignment
682	670–691	1st order A_2
806	774–775	1st order A_2
854	870–876	1st order E_1
915	905	2nd order[b] $2E_{25}(262 + 643)(15, 0)$
956	970	2nd order[b] $2E_{25}(295 + 675)(15, 0)$
987	970	2nd order[b] $2E_{25}(295 + 675)(15, 0)$
1033	1034	2nd order[b] $2A_1(346 + 688)(10, 10)$
1095	1110–1130	2nd order[b] $2E_9(432 + 681)(10, 10)$, $2E_{19}(525 + 605)(15, 0)$, $2E_{10}(443 + 670)(14, 7)$
1164	1110–1130	2nd order[b] $2E_9(432 + 681)(10, 10)$, $2E_{19}(525 + 605)(15, 0)$, $2E_{10}(443 + 670)(14, 7)$
1197	1110–1130	2nd order[b] $2E_9(432 + 681)(10, 10)$, $2E_{19}(525 + 605)(15, 0)$, $2E_{10}(443 + 670)(14, 7)$
1262	1248–1261	1st order A_2
1369	1365–1370	1st order A_2
1443	1455	2nd order[b] $2E_{12}(338 + 1117)(10, 10)$, $2E_6(343, 1112)(15, 0)$, $2E_9(765 + 692)(14, 7)$
1541	1499–1501	1st order A_2
1564	1582–1588	1st order E_1
1585	1582–1588	1st order E_1
1708	1710–1750	2nd order[b] $2A_1(859 + 859)(10, 10)$, $2E6(339 + 1406)(15, 0)$, $2E_7(681 + 1029)$ and $2E_{21}(159 + 1551)(14, 7)$
1730	1710–1750	2nd order[b] $2A_1(859 + 859)(10, 10)$, $2E6(339 + 1406)(15, 0)$, $2E_7(681 + 1029)$ and $2E_{21}(159 + 1551)(14, 7)$

[a]Purified sample HTVA = 1400 °C (c.f. Figs. 1 and 2).
[b]Based on JDOS for (10,10),(15,0),(14,7).

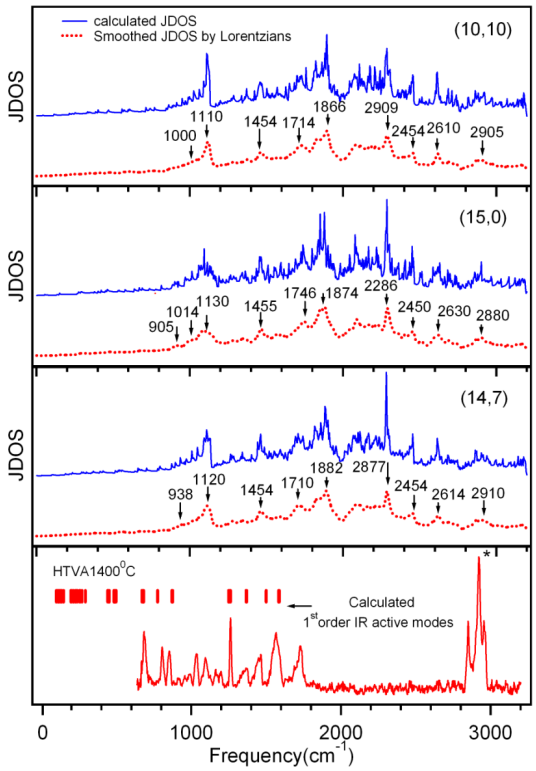

FIG. 3 (color online). Top three panels: calculated 2-phonon DOS for three selected tubes [(10,10), (15,0), (14,7)]. Bottom panel: experimental IR spectrum (HTVA = 1400 °C).

Γ and M points of the BZ. Details of our phonon calculations are given in Ref. [4]. The small differences we observe with diameter (Fig. 2, upper set of vertical bars) are perhaps not significant at the moment, amounting to a scatter as a function of diameter for nanotubes that is $\sim 10\ \mathrm{cm}^{-1}$. This scatter is comparable to the FWHMs of the features in Fig. 2.

Finally, we should also consider possible 2nd order SWNT features that might be observed in the IR spectrum. Two-phonon IR absorption can occur at a frequency $\omega(q) = \omega_1(q_1) \pm \omega_2(q_2)$, where the ω_j are the phonon frequencies; the total wave vector of the two-phonon excitation must satisfy $q = q_1 + q_2 = 0$. Here, we only consider the case where two phonons are created ($\omega = \omega_1 + \omega_2$). In one-dimensional materials, we can also expect vHs in the one- and two-phonon density of states. Thus 2-phonon excitations involving vHS could also lead to sharp structures in the IR spectrum.

In Fig. 3, we compare our calculated 2-phonon DOS (JDOS) for three selected tubes (top three curves) with the experimental IR spectrum. The vertical bars above the experimental spectrum (bottom) locate the calculated IR-active one-phonon frequencies. Note that the three tubes chosen for Fig. 3 are from the three families (n, n), $(n, 0)$, and (n, m) $n \neq m$. Despite the difference in chirality, the JDOS for these three tubes exhibits considerable similarity. It should also be noted that two curves are present for each JDOS: the solid curve is the JDOS (as calculated), and the dotted curve is the JDOS smoothed by a convolution with a Lorentzian. The latter is done to mimic the effects of a moderately short phonon lifetime (0.1 ps) [26]. From the smoothed JDOS shown in the figure, we can say that the three different symmetry tubes chosen all provide a large 2-phonon DOS near $\sim$1110–1130 cm^{-1}, $\sim$1455 cm^{-1}, $\sim$1710–1750 cm^{-1}, in agreement with experiment (c.f., Table I).

In conclusion, we have studied the evolution of the IR spectrum of purified SWNT samples that were vacuum annealed to high temperatures (up to 1400 °C). The higher temperatures should remove all chemical functional groups. Through comparison with theory, 8 out of the 18 IR bands that remain in samples annealed in the range 1100 °C–1400 °C can be assigned to first order IR modes (A_2 or E_1). The remaining 10 bands are assigned to two-phonon excitations.

This work was supported, in part, by the National Science Foundation NSF-DMR-0103585 (PSU), NSF-DMR-0304178 (PSU), NSF-DMR-04-05538 (MIT). C. A. F. acknowledges financial support from CNPq-Brazil. R. S. acknowledges a Grant-in-Aid (No. 13440091 and No. 16076201) from the Ministry of Education, Japan. We thank Professor G. D. Mahan and V. H. Crespi, for helpful discussions.

*To whom correspondence should be addressed.
Electronic address: pce3@psu.edu

[1] N. Hamada *et al.*, Phys. Rev. Lett. **68**, 1579 (1992).
[2] J. W. Mintmire *et al.*, Phys. Rev. Lett. **68**, 631 (1992).
[3] R. Saito *et al.*, Appl. Phys. Lett. **60**, 2204 (1992).
[4] R. Saito, G. Dresselhaus, and M. S. Dresselhaus, *Physical Properties of Carbon Nanotubes* (Imperial College Press, London, 1998).
[5] A. M. Rao *et al.*, Science **275**, 187 (1997).
[6] A. Pimenta *et al.*, Phys. Rev. B **58**, R16016 (1998).
[7] H. Qiu *et al.*, Nano Lett. **5**, 749 (2005).
[8] Kane *et al.*, Phys. Rev. Lett. **90**, 207401 (2003).
[9] D. Spataru *et al.*, Phys. Rev. Lett. **92**, 077402 (2004).
[10] Perebeinos *et al.*, Phys. Rev. Lett. **92**, 257402 (2004).
[11] Kuhlmann *et al.*, Chem. Phys. Lett. **294**, 237 (1998).
[12] Furtado *et al.*, J. Am. Chem. Soc. **126**, 6095 (2004).
[13] R. A. Jishi *et al.*, Chem. Phys. Lett. **209**, 77 (1993).
[14] R. A. Jishi *et al.*, Phys. Rev. B **47**, 16 671 (1993).
[15] Damnjanovic *et al.*, Phys. Rev. B **60**, 2728 (1999).
[16] U. J. Kim *et al.* J. Am. Chem. Soc. (to be published).
[17] K. Kamaras *et al.*, Science **301**, 1501 (2003).
[18] R. Saito *et al.*, Phys. Rev. B **46**, 1804 (1992).
[19] H. Kataura *et al.*, Synth. Met. **103**, 2555 (1999).
[20] E. A. Taft *et al.*, Phys. Rev. **138**, A197 (1965).
[21] B. N. Khare *et al.*, Nano Lett. **2**, 73 (2002).
[22] J. Jiang *et al.*, Phys. Rev. B **71**, 045417 (2005).
[23] Souza Filho *et al.*, Phys. Rev. B **65**, 035404 (2002).
[24] Souza *et al.*, Phys. Rev. B **69**, 241403 (2004).
[25] Maultzsch *et al.*, Phys. Rev. Lett. **92**, 075501 (2004).
[26] J-S. Lauret *et al.*, Phys. Rev. Lett. **90**, 057404 (2003).